Arch. Metall. Mater., Vol. 61 (2016), No 2, p. 811–820

DOI: 10.1515/amm-2016-0137

A. GRAJCAR*,#, D. WOŹNIAK**, A. KOZŁOWSKA*

NON-METALLIC INCLUSIONS AND HOT-WORKING BEHAVIOUR OF ADVANCED HIGH-STRENGTH MEDIUM-Mn STEELS

The work addresses the production of medium-Mn steels with an increased Al content. The special attention is focused on the identification of non-metallic inclusions and their modification using rare earth elements. The conditions of the thermomechanical treatment using the metallurgical Gleeble simulator and the semi-industrial hot rolling line were designed for steels containing 3 and 5% Mn. Hot-working conditions and controlled cooling strategies with the isothermal holding of steel at 400°C were selected. The effect of Mn content on the hot-working behaviour and microstructure of steel was addressed. The force-energetic parameters of hot rolling were determined. The identification of structural constituents was performed using light microscopy and scanning electron microscopy methods. The addition of rare earth elements led to the total modification of non-metallic inclusions, i.e., they replaced Mn and Al forming complex oxysulphides. The Mn content in a range between 3 and 5% does not affect the inclusion type and the hot-working behaviour. In contrast, it was found that Mn has a significant effect on a microstructure.

Keywords: medium-Mn steel, steel cleanliness, non-metallic inclusions, bainitic steel, hot rolling, retained austenite.

1. Introduction

Advanced high-strength steels (AHSS) for the automotive industry combine high strength levels and exceptional ductility levels compared to conventional high-strength low-alloyed (HSLA) steels with limited plasticity at room temperature. The 1st generation of AHSS characterized by multiphase microstructures is successfully used in cars for about 10 years. Their application resulted in the improvement of crashworthiness of cars and reduction of the weight of body-in-white. Generally, the combination of high strength and ductility is caused by high work hardening rates of multiphase steels as an effect of the interaction between hard and soft microstructural constituents [1-3]. Additionally, the plasticity is enhanced by strain-induced martensitic transformation of retained austenite especially in TRansformation Induced Plasticity (TRIP) steels [3-6]. Even better ductility levels can be obtained for the 2nd generation of AHSS showing a pure austenitic microstructure because of high manganese additions (from 20 to 30 wt.%). These steels are strengthened by TRIP effect or intense mechanical twinning, which is known as a TWIP (Twinning Induced Plasticity) effect [7-10]. However, the cost penalty because of high-Mn content and other alloying elements (~ 3% Si and Al) is the main disadvantage of their industrial application.

The 3rd generation of AHSS include medium-Mn steels (between 3-12 wt.%), in which the high amount of retained austenite (between 15 and 40 vol.%) is embedded in a fine-grained or ultra fine-grained ferrite or a mixture of ferrite and bainite. The optimum utilization of the TRIP and TWIP effects allows to obtain a similar strength-ductility balance like for the high-Mn alloys but at reduced cost. These are the reasons of intense world-wide research on relationships between heat treatment, microstructure and mechanical properties of medium-Mn steels [11-13]. Their microstructure is similar to that observed in nano-size bainite-austenite steels, in which the γ phase is enriched in C during an isothermal bainite transformation [14-16]. Sometimes, the enrichment of austenite in carbon proceeds from martensite in so-called QP (quenching and partitioning) steels [17, 18]. In medium-Mn steels the stability of retained austenite to room temperature is usually obtained by its enrichment both in C and Mn following intercritical annealling in the $\gamma+\alpha$ range [11].

In contrast to numerous reasearch on microstructure-property relationships, a metallurgical cleanliness of medium-Mn steels have not attracted the noticable attention so far. These steels contain increased manganese and aluminium contents. Thus, the formation of numerous sulphides and oxides affecting mechanical and technological properties should be expected. It is well known that these inclusions deteriorate formability, weldability, crack resistance etc. [19]. Unfortunately, there are only a few works on characterization of non-metallic inclusions in advanced high-strength steels with increased Mn content [20, 21]. Therefore, the first part of the present work is focused on the determination of non-metallic inclusions types in selected medium-Mn steels.

The successful industrial production of AHSS requires the knowledge of their hot-working behaviour. Physical simulation [10, 17, 22-25] and numerical modelling [26-29] are the effective ways of determining the force-energetic parameters

* SILESIAN UNIVERSITY OF TECHNOLOGY, INSTITUTE OF ENGINEERING MATERIALS AND BIOMATERIALS, 18A KONARSKIEGO STR., 44-100 GLIWICE, POLAND

** INSTITUTE FOR FERROUS METALLURGY, 12-14 K. MIARKI STREET, 44-100 GLIWICE, POLAND

Corresponding author: adam.grajcar@polsl.pl

and microstructure evolution during thermomechanical processing. The hot-working behaviour is rarely investigated using semi-industrial hot-rolling lines [9, 30, 31] or on the basis of real industrial rolling trials [26, 32]. In semi-industrial conditions rolling forces and mean flow stresses are monitored to determine thermally activated processes occuring during hot deformation. Recently, Poliak and Bhattacharya [33] reviewed some aspects of thermomechanical processing of third generation advanced high-strength steels. Following our previous studies on physical modelling of medium-Mn steels under labaratory conditions [12, 13, 24], the present work aims to shed some light on hot-working behaviour of these 3rd generation medium-Mn AHSS using a semi-industrial hot strip rolling line.

2. Experimental

2.1. Alloy preparation

The chemical composition of the developed medium-Mn steels is given in Table 1. The two alloys differ in the manganese content, which is a basis for steel designation (3Mn-1.5Al-Nb and 5Mn-1.5Al-Nb). The carbon content is limited to 0.17 wt.% because of welding reasons whereas Mn is added to increase the fraction of austenitic phase. Aluminium concentration of approximately 1.5% should suppress carbide precipitation [3, 11]. Molybdenum and niobium additions were added in order to increase strength properties. The ingots were produced using vacuum induction melting and hot forging to a thickness of 22 mm. The samples with a diameter of 10 mm and a height of 12 mm were machined for axisymmetrical compression tests. Subsequently, the flat samples were roughly rolled to a thickness of approximately 8.5 mm. The final hot-working experiments consisted of thermomechanical rolling of 8.5 mm thick specimens in five passes to sheets with a thickness of approximately 3.3 mm.

The steel charge consisted of Armco iron and pure additions of C, Si, Mn, Mo, Al as well as Fe-Nb ferroalloys. Fe and Mo were loaded into the crucible while the alloying elements were distributed into individual compartments of the hopper in the order (Al, Si, Mn, C, Fe-Nb) corresponding to their addition into the liquid metal. The mischmetal (~50%Ce, ~20%La, ~20%Nd) was added to modify non-metallic inclusions. The amount of rare earth elements (REE) was equal to 2 g per 1 kg of charge. This addition should modify a chemical composition of inclusions due to the high chemical affinity of Ce, La and Nd to oxygen and sulphur. The oxides and sulphides of RE elements are thermally stable at high temperatures of hot-working and have the small tendency to deform along the rolling direction [20, 21]. Therefore, the limitation of the anisotropy of mechanical properties of sheets is expected. The liquid steel was cast under Ar protection from 1545°C into a 25 kg hot-topped closed-bottom cast iron mould.

2.2. Multi-step compression test

The four-step compression test was carried out to study the effect of such deformation on the hot-working behaviour

TABLE 1

Chemical composition of the investigated steels (wt. %)

Steel grade	C	Mn	Al	Si	Mo	Nb	S	P	O	N
3Mn-1.5Al-Nb	0.17	3.1	1.6	0.22	0.22	0.04	0.005	0.008	0.0006	0.0046
5Mn-1.5Al-Nb	0.17	5.0	1.5	0.21	0.20	0.03	0.005	0.008	0.0004	0.0054

TABLE 2

Parameters of the four-step compression test and cooling conditions of axisymmetrical samples deformed using the Gleeble simulator

Heating					
Soaking temperature, °C		Heating rate, °C/s	Soaking time, s	Cooling rate to deformation temperature, °C/s	
1200		3	30	5	
Deformation conditions					
No.	T, °C	ε	$\dot{\varepsilon}$, s^{-1}	Cooling rate to a successive deformation step, °C/s	Time between successive deformation steps, s
1	1150	0.25	10	8	12.5
2	1050	0.25	10	10	10
3	950	0.25	10	10	10
4	850	0.25	10	below	–

Cooling conditions after deformation						
	Temperature range, °C		Cooling rate, °C/s		Isothermal holding time, s	
	3Mn-1.5Al-Nb	5Mn-1.5Al-Nb	3Mn-1.5Al-Nb	5Mn-1.5Al-Nb	3Mn-1.5Al-Nb	5Mn-1.5Al-Nb
1	850 → 700	850 → 400	$v_1 = 40$	v = 40	–	–
2	700 → 650		$v_2 = 1$		–	
3	650 → 400		$v_3 = 40$		–	
4	400	400	–	–	300	300
5	400 → 20	400 → 20	0.5	0.5	–	–

and subsequent phase transformations of deformed austenite. The hot deformation and cooling routes are illustrated in Fig. 1a whereas the detailed parameters of heating, deformation and cooling are listed in Table 2.

The hot compression tests were performed using the DSI Gleeble 3800 thermomechanical simulator. The specimens were resistance-heated in vacuum to 1200°C and soaked within 30 s. The hot-working included four compression steps at decreasing temperatures 1150, 1050, 950 and 850°C. The true strain values were equal to 0.25 at a strain rate of $10s^{-1}$.

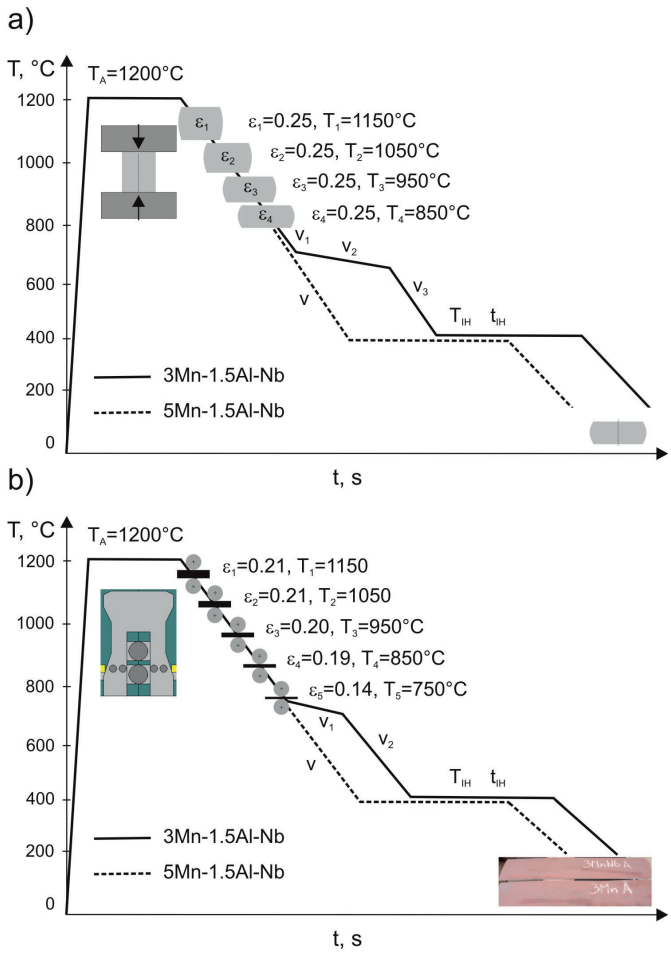

Fig. 1. Schematic of the deformation schedules and cooling conditions for the samples deformed in the Gleeble simulator (a) and thermomechanically rolled to a thickness of 3.3 mm (b); T_A – austenitizing temperature, v – cooling rate, T_{IH} – isothermal holding temperature, t_{IH} – isothermal holding time

The cooling path following the final deformation step at 850°C varied on the steel grade. The 3Mn-1.5Al-Nb steel was initially quickly cooled to 700°C (v_1) and subsequently slowly cooled at a rate of 1°C/s (v_2) from 700°C to 650°C to initiate the γ→α transformation. After that the samples were again fast cooled (v_3) to 400°C and isothermally held at this temperature within 300 s to form bainite and enrich austenite in carbon. Air cooling was the last cooling step. The cooling path of the steel that contains 5% Mn was more simple (Fig. 1a). The aim was to obtain a mixture of bainite and retained austenite. Therefore, the samples were immediately cooled at a rate of v = 40°C/s to a temperature of 400°C.

2.3. Semi-industrial thermomechanical processing

The thermomechanical processing tests were performed using the semi-industrial hot-rolling line (LPS) at the Institute for Ferrous Metallurgy (Gliwice, Poland). The detailed description of the line can be found elsewhere [30]. The experiment aimed to simulate a real industrial technological process of hot strip rolling. Before hot-rolling trials, flow stresses (σ_p) have been calculated according to the Hensel-Spittel equation [34]:

$$\sigma_p = \sigma_0 \cdot k_T \cdot k_\varepsilon \cdot k_{\dot{\varepsilon}} \quad (1)$$

where:
σ_0 – initial yield stress,
k_T – temperature effect coefficient,
k_ε – strain effect coefficient,
$k_{\dot{\varepsilon}}$ – strain rate effect coefficient.

The next important parameter, which describes the rolling mill load, is the mean unit pressure (p_{mean}). A majority of theoretical equations is calculated on the basis of the equilibrium condition of forces acting on an infinitesimal element, separated in the roll gap. The best results for the applied D550 two-high rolling mill can be obtained for the Zjuzin method [35]. The mean unit pressure can be calculated as follows:

$$p_{mean} = n_b \cdot n_\sigma \cdot \sigma_p \quad (2)$$

where:
n_b – strip width effect coefficient,
n_σ – stress state coefficient,
σ_p – flow stress determined on the basis of the rolled strip temperature.

The advantage of the calculation of mean unit pressure according to the applied method is the consideration of the present stress state and strip width depending on the coefficient of roll gap shape.

The hot-rolling tests were conducted in five passes between 1200 °C and 750 °C to a final sheet thickness of approximately 3.3 mm. The deformation and cooling paths are schematically drawn in Fig. 1b whereas the detailed parameters of the process are given in Table 3. The strain values were slightly lower compared to the Gleeble experiments because of high rolling forces measured whereas the strain rate increased for each next pass reaching a value close to $10\ s^{-1}$, that is similar to the one applied in the thermomechanical simulator. The temperature of the following passes was registered before and after a rolling stand using stationary pyrometers. Additionally, the rolling temperature was measured using a portable pyrometer.

The cooling conditions following hot rolling were very similar to these ones applied using the Gleeble simulator. The differences for the 3Mn-1.5Al-Nb steel include the shortening of the time of slow cooling of sheet samples in the γ→α transformation region, i.e, between 750°C and 700°C (Table 3). The cooling rate from 700°C to the isothermal holding temperature of 400°C was decreased from 40°C/s to

TABLE 3

Parameters of the thermomechanical rolling of samples to a final sheet thickness of 3.3 mm using the semi-industrial rolling line

Rolling conditions						
No.	T, °C	ε	$\dot{\varepsilon}$, s^{-1}	Sheet thickness after a pass, mm		Time between successive passes, s
1	1150	0.21	4.4	6.9		15
2	1050	0.21	5.7	5.6		12
3	950	0.20	7.0	4.6		10
4	850	0.19	8.6	3.8		8
5	750	0.14	7.7	3.3		–
Cooling conditions after hot rolling						
	Temperature range, °C		Cooling rate, °C/s		Isothermal holding time, s	
	3Mn-1.5Al-Nb	5Mn-1.5Al-Nb	3Mn-1.5Al-Nb	5Mn-1.5Al-Nb	3Mn-1.5Al-Nb	5Mn-1.5Al-Nb
1	750 → 700	750 → 400	$v_1 = 10$	v = 27	–	
2	700 → 400		$v_2 = 27$		–	
3	400	400	–	–	300	300
4	400 → 20	400 → 20	air	air	–	–

about 27°C/s. The mixed air-blow and water-spray cooling devices were applied. The mentioned changes better reflect real industrial conditions. The 5Mn-1.5Al-Nb steel samples were directly cooled to 400°C after the last pass at 750°C (Fig. 1b).

2.4. Metallographic investigations

Metallographic specimens were taken along the rolling direction. The polished specimens were prepared to identify non-metallic inclusions whereas the second group of specimens was etched in order to reveal the microstructure. A chemical composition of non-metallic inclusions was identified using the JCXA 8230 X-ray microanalyser at the accelerating voltage of 15 kV and the current of 30 nA. Qualitative examination of the chemical composition of inclusions was performed using the energy-dispersive spectroscopy whereas distribution maps of alloying elements were analysed using the wavelength-dispersive spectrometry method.

Light microscopy (LM) and scanning electron microscopy (SEM) were used to analyse the microstructure. Nital etching and 10% aqueous solution of sodium metabisulfite were used. Metallographic observations were performed with a Leica MEF 4A light microscope. The morphological details of the microstructural constituents were revealed with the SUPRA 25 SEM using back-scattered electrons.

3. Results and discussion

3.1. Non-metallic inclusions

The analysis of non-metallic inclusions was carried out for the specimens after the thermomechanical rolling. The representative images showing the distribution of the non-metallic inclusions in the 3Mn-1.5Al-Nb steel and 5Mn-1.5Al-Nb steel are presented in Fig. 2. As expected, there are no significant differences between the two alloys investigated, since the sulphur contents are at a level of 0.005 wt.% in both steels. It means that the increase of the Mn addition from 3 to 5 wt.% does not affect considerably the amount, distribution and size of particles.

Fig. 2. Non-metallic inclusions after the thermomechanical rolling at the longitudinal section revealed in the 3Mn-1.5Al-Nb steel (a) and 5Mn-1.5Al-Nb steel (b)

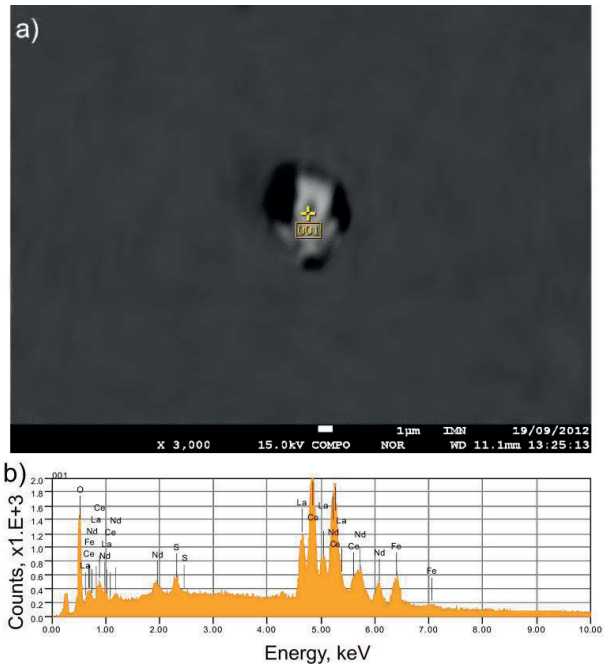

Fig. 3. The complex oxysulphide of rare earth elements identified in the 3Mn-1.5Al-Nb steel (a) and the corresponding EDS spectrum from the point 001 (b)

The identified inclusions have a various size and a morphology. There are numerous small equiaxed particles and some larger inclusions located individually or forming agglomerations. The larger inclusions forming chains are usually preferentially oriented along the rolling direction but they deform to a very limited extent. The detailed quantitative measurements [21] revealed that the mean aspect ratio ranges from 1.45 to 1.6. The fraction of non-metallic inclusions in the investigated steels is in a range from 0.12 to 0.18%. It is interesting to note that the fraction of particles in the same medium-Mn steels not subjected to the mischmetal treatment is twice larger. It means that the RE elements effectively reduce both the volume fraction of inclusions and their deformability. The average area of particles is from 9 to 13 μm^2 independently on the Mn content.

The explanation of the low tendency of the non-metallic inclusions to elongate can be the analysis of their chemical composition. The micrograph in Fig. 3 shows a typical particle with a diameter of approximately 5 µm identified in the steel containing 3% Mn. It is interesting that the spectrum in Fig. 3b does not contain any spectral lines from Fe, Si, Al and Mn. Instead of them there is a clear signal from Ce, La, and Nd. The confirmation are the elemental maps of various elements shown in Fig. 4. It is clear that the RE elements are located homogeneously through the entire particle. These elements have the higher chemical affinity to oxygen and sulphur [21, 36]. Therefore, they replaced Mn in sulphide inclusions and Al in alumina dendrites forming complex RE oxysulphides.

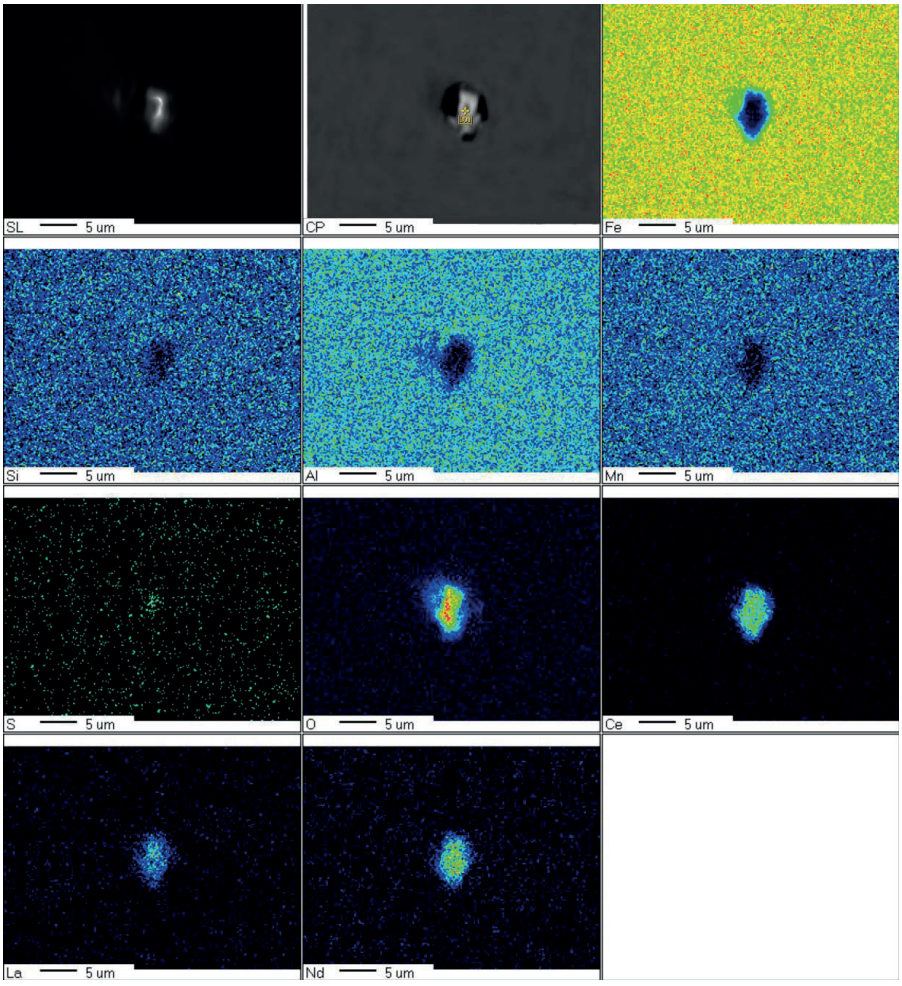

Fig. 4. Maps of elements forming the complex oxysulphide from Fig. 3 in the 3Mn-1.5Al-Nb steel

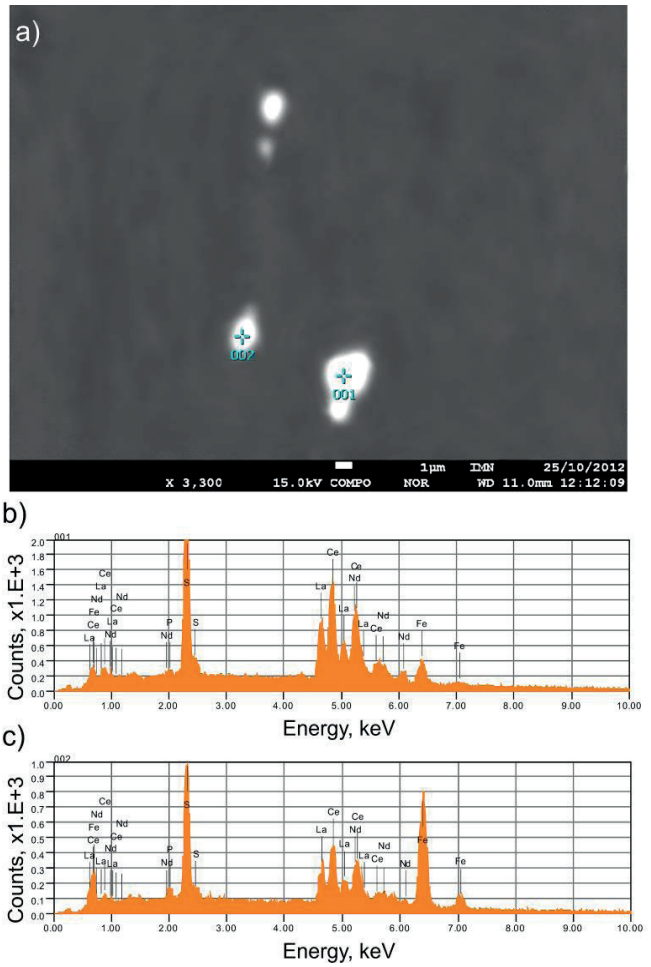

Fig. 5. The complex sulphide of rare earth elements identified in the 5Mn-1.5Al-Nb steel (a) and the corresponding EDS spectra from the points 001 (b) and 002 (c)

The increase of manganese concentration to 5% does not change the chemical composition of identified particles. Figure 5a shows the micrograph of the 5Mn-1.5Al-Nb steel, which contains a few equiaxed particles with a size ranging from 1 to 4 µm. It should be noted there are no spectral lines from Mn, Al and Si too. Manganese is only present in the largest deformed inclusions whereas aluminium forms small nitrides [21]. There are no distinct differences of the chemical composition between larger and smaller inclusions (Fig. 5b and Fig. 5c). The mapping of the particles in Fig. 6 indicates that they are composed of rare earth elements and sulphur. The particles are totally modified by RE elements, which means that the mischmetal addition of 2 g per 1 kg of steel is efficient in terms of the modification of non-metallic inclusions in medium-Mn Al-alloyed steels.

3.2. Gleeble simulations

The hot deformation response from four-step compression tests is presented in Fig. 7. The flow stresses increase significantly with decreasing deformation temperature, ranging from 125 MPa at 1150°C to 275 MPa at a final deformation temperature of 850°C. All the curves show a rapid increase of stress with increasing strain at the successive deformation steps. This behaviour is typical for the alloys in which the hot deformation is controlled by dynamic recovery, i.e., any peaks related to dynamic recrystallization can be distinguished in the curves. The dislocations generated during plastic deformation are partially removed by thermally activated processes including the cross slip of screw dislocations and climb of edge dislocations.

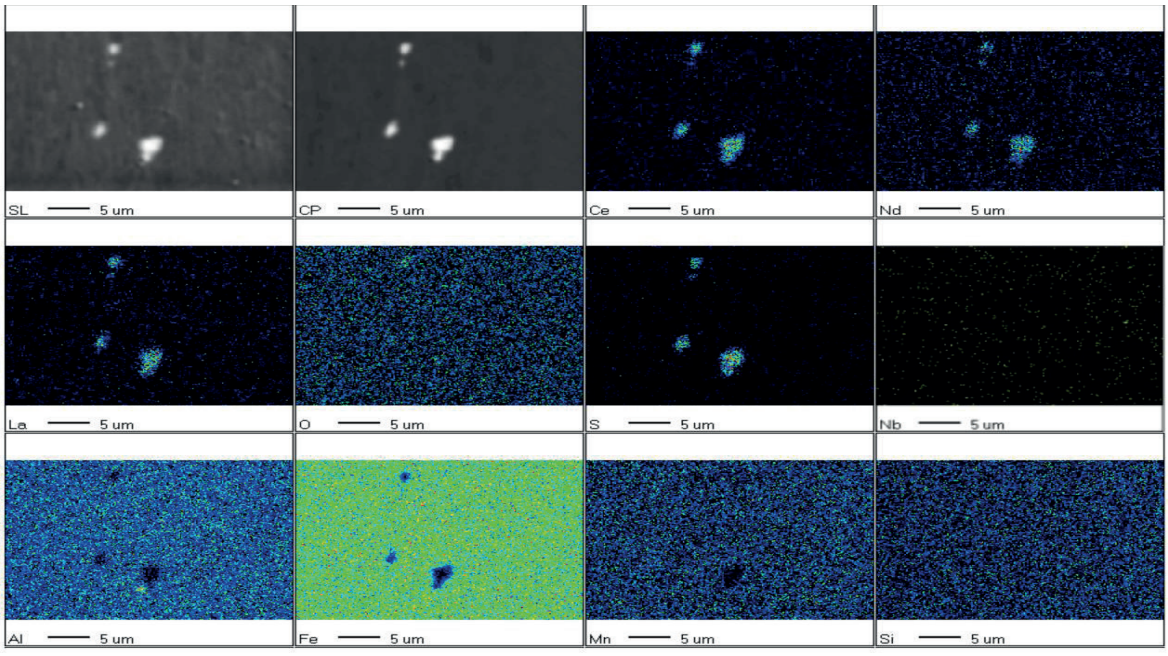

Fig. 6. Maps of elements forming the complex sulphides from Fig. 5 in the 5Mn-1.5Al-Nb steel

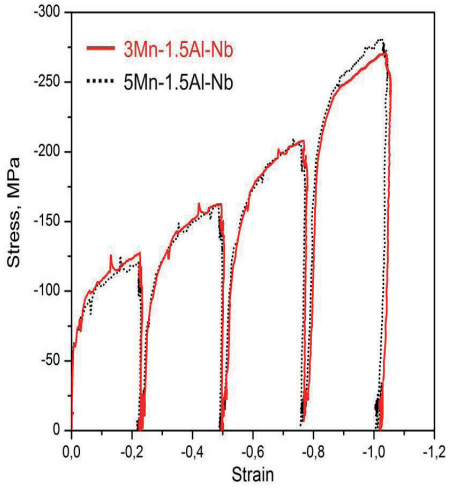

Fig. 7. Comparison of hot deformation response from a hot compression test performed in a temperature range between 1150°C and 850°C at strain rate of $10s^{-1}$ and strain value of 0.25

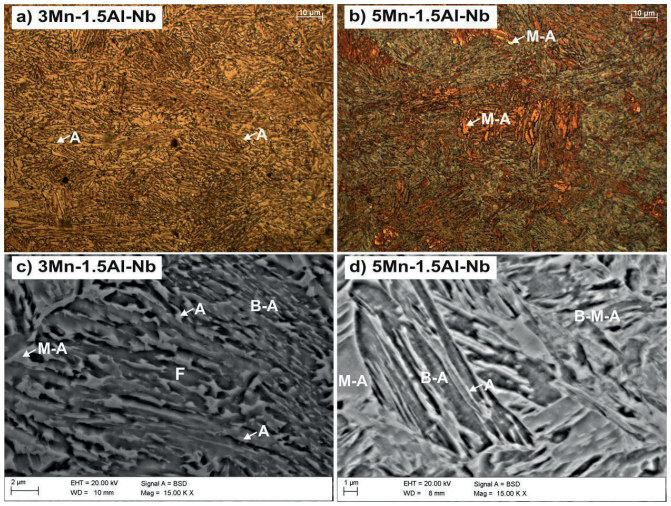

Fig. 8. LM microstructures (a, b) and SEM microstructures (c, d) of the investigated steels thermomechanically processed using the four compression test; A – retained austenite, M-A – martensite-austenite constituents, F – ferrite, B-A – bainite-austenite constituents, B-M-A – bainite-martensite-austenite regions

The interval times between the compression steps were equal to about 10 s (Table 2). On the basis of our earlier investigations [12, 24] it can be concluded that the progress of the static recrystallization between compression passes is limited to approximately 20-40% depending on the deformation temperature. It means that the strong strain accumulation occurs from one pass to another pass. In industrial hot strip rolling this can lead to the initiation of dynamic recrystallization in final passes at decreasing temperatures [33]. It is not a case for the investigated steels due to smaller number of passes and lower reductions applied.

It appears that the strongest rise of the stress takes place between the third and fourth deformation steps. This behaviour is presumably related to the deformation of the austenite below the non-recrystallization temperature [23, 25]. The interesting effect is that the flow stress values in Fig. 7 are very similar for both steels. It means that the addition of manganese from 3 to 5% does not affect the hot-working behaviour of the investigated alloys. The same effect was observed by Grajcar et al. [24] during continuous compression tests. The registered flow stresses are higher compared to the values reported for conventional DP and TRIP steels containing the Mn content usually limited to approximately 2%. For example, Adamczyk et al. [4] reported the values of flow stresses lower than 250 MPa for 0.23C-1.5Mn-0.8Al-0.2Si-0.2Cr TRIP steel subjected to the plane strain compression. Lin et al. [27] registered stresses below 200 MPa at a final deformation temperature of 890°C for the 0.19C-1.5Mn-1.6Si-0.2Mo steel subjected to the multi-step torsion. A sharp increase of the stress value took place at about 950°C. The similar effect can be indicated in Fig. 7. It should be noted that in such analyses the deformation method, deformation conditions (strain value, strain rate, interpass time) affect results significantly. The effect of strain rate is very important since the parameter reaches 100-150 s^{-1} in final passes of hot strip rolling processing [33].

The confirmation of the strong strain accumulation in the austenite prior to cooling using the Gleeble simulator are the micrographs of the thermomechanically processed samples in Fig. 8. Light microscopy images show that both steels are characterized by significant grain refinement (Fig. 8a, b). The steels have strong hardenability due to Mn addition and thus needle-like microstructures typical for low-temperature products of austenite transformation. The amount of ferrite is negligible in the 3Mn-1.5Al-Nb steel even after the slow cooling of steel within 50 s between 700°C and 650°C (Fig. 8a). The morphology of structural constituents can be assessed after applying SEM. Bainite is a major constituent of the steel containing 3% Mn. Isothermal holding of steel at 400°C results in the incomplete bainite reaction phenomenon [2, 3], which is supported by the addition of Al. As a result cementite precipitation is prevented and carbide particles are replaced by retained austenite layers located between bainitic ferrite laths (Fig. 8c). The bainite is the major phase of the 5Mn-1.5Al-Nb steel too. However, numerous blocky austenite grains transformed into martensite upon cooling forming martensite-austenite constituents (Fig. 8d). Therefore, the steel with the higher Mn concentration contains some portion of martensite and a smaller fraction of retained austenite than the 3Mn-1.5Al-Nb steel.

According to earlier research by Grajcar and Kwaśny [37] the amount of retained austenite (determined by X-ray diffraction) in the steel containing 3% Mn is 18.4% whereas it is equal to 11.2% in the steel with the higher Mn concentration. It is interesting since manganese is an austenite stabilizer. However, the present data are in accordance with the experimental data recently reported by Sugimoto et al. [38] for medium-Mn steels containing from 1.5 to 5% Mn. They reported that the most important indicator of the stability of retained austenite is a C content in the γ phase. According to the thermodynamic calculations the carbon content in the austenite decreases with the increase in the Mn concentration. This behaviour was observed in [38] and our results confirmed this effect. The C content of the 3Mn-1.5Al-Nb reaches 1.12% and decreases to 0.77% [37] with the increase of Mn concentration to 5%.

3.3. Thermomechanical rolling

The calculated and measured parameters of the thermomechanical rolling of flat samples to a final sheet thickness of 3.3 mm using the semi-industrial rolling line are summarized in Table 4. The graphical illustration of flow stress and mean unit pressure calculated for successive passes is presented in Fig. 9 for the 5Mn-1.5Al-Nb steel. Similarly like in case of the hot compression tests the results for both steels are almost the same. One can see a clear dependence between a pass number and corresponding force-energetic parameters. Both flow stress and mean unit pressure increase with decreasing the temperature from one pass to another. The same tendency concerns the roll loads (Table 4). The comparison of the calculated values of roll loads with the measured ones indicates clearly that the difference does not exceed 5%. It means that the methodology of the determination of the force-energetic parameters of hot-rolling is very satisfactory.

Poliak and Bhattacharya [33] reported that different AHSS have higher deformation resistance and resulting roll forces than C-Mn and microalloyed grades due to richer alloying. Moreover, traditional thermomechanical processing strategies (recrystallization controlled rolling and no-recrystallization controlled rolling) can not be fully realized in industrial finishing rolling of AHSS due to delayed initiation of static recrystallization. It should be noted that the present conditions differ from the industrial ones in number of passes, reductions, strain rates etc. Therefore, the flow stresses during hot rolling (Fig. 9) of the investigated steels are significantly smaller when compared to the values registered for the hot-compressed samples (Fig. 7). It is a result of the different stress state during hot rolling and axisymmetrical compression and smaller reductions applied during thermomechanical rolling.

TABLE 4

Calculated and measured values corresponding to the thermomechanical rolling of samples to a final sheet thickness of 3.3 mm using the semi-industrial rolling line

Pass no.	Calculated values			Measured values
	Flow stress, MPa	Mean unit pressure, MPa	Roll load, kN	Roll load, kN
1	108.0	241.7	1019	990
2	116.9	308.7	1108	1120
3	127.0	388.8	1157	1200
4	138.9	482.2	1173	1230
5	156.8	618.8	1257	1310

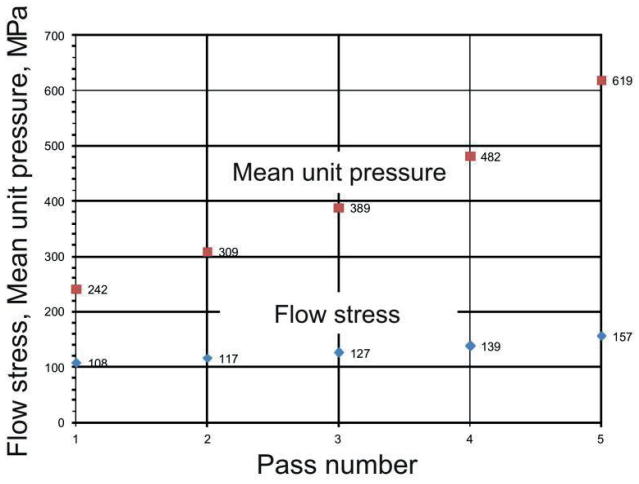

Fig. 9. Results of calculated values of flow stress and mean unit pressure for the 5Mn-1.5Al-Nb steel in successive passes of the hot rolling

The microstructures produced after the thermomechanical rolling are shown in Fig. 11. Both the degree of grain refinement and the type of structural constituents are very similar to the ones obtained in the Gleeble simulator. It means that the main hot deformation conditions and cooling paths applied during the semi-industrial hot-rolling reflect good laboratory conditions.

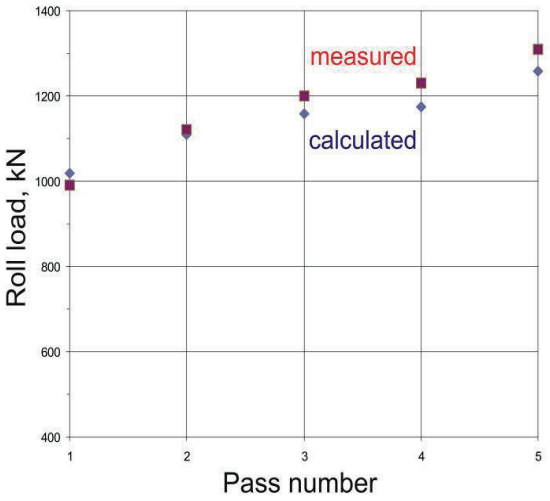

Fig. 10. Comparison of calculated and measured values of roll loads in successive passes of the hot rolling for the 5Mn-1.5Al-Nb steel

One can see that the bainitic-austenitic and bainitic-martensitic-austenitic mixtures are more elongated along the rolling direction (Fig. 11a, b). It is because of the additional rolling pass and thus the lower finishing deformation temperature of approximately 750°C. A higher amount of M-A constituents in the 3Mn-1.5Al-Nb steel can be also visible in Fig. 11c. The major reason is presumably related to the reduction

of the cooling rate to the isothermal holding temperature from 40°C/s to 27°C/s. The volume fraction of retained austenite is again higher for the steel containing the lower Mn content. It is associated with the difference in carbon enrichment of the γ phase depending on the manganese concentration.

Grajcar et al. [31] reported that the amount of retained austenite in the 3Mn-1.5Al-Nb steel is equal to 15.5% and decreases to 8.3% for the steel containing 5% Mn. The carbon contents in the austenite are similar like for the previously described samples treated using the Gleeble simulator. It seems that the Mn content of 3% is a critical value for producing a reasonable volume fraction of retained austenite in medium-Mn steels treated from the hot-working region. The higher fractions of retained austenite in steels containing between 4 and 12% Mn can be only stabilized by intercritical annealing of steels. Under such conditions the austenite is stabilized both by C and Mn [11].

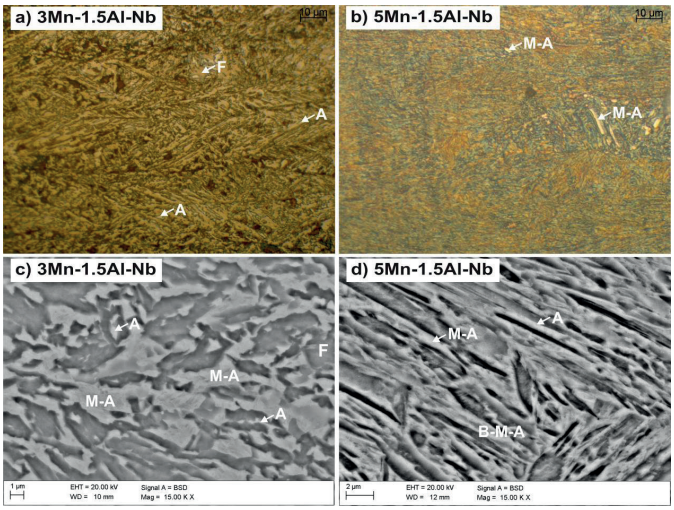

Fig. 11. LM microstructures (a, b) and SEM microstructures (c, d) of the investigated steels thermomechanically processed using the semi-industrial hot-rolling line; A – retained austenite, M-A – martensite-austenite constituents, F – ferrite, B-M-A – bainite-martensite-austenite regions

4. Conclusions

The medium-Mn steels are a new group of advanced ferrous alloys for the automotive industry for which the challenging steelmaking processes and thermomechanical rolling practices are required. The monitoring of the type and morphology of non-metallic inclusions in steels with increased Mn and Al additions is very important. The mischmetal addition proves as a very efficient compound to modify the chemical composition of the produced steels containing 1.5% Al and Mn in a range from 3 to 5%. The REE totally replaced Mn and Al in identified sulphides and oxysulphides of the low tendency to elongate along the rolling direction. The high steel cleanliness and the selection of proper hot deformation and cooling strategies allow to produce the high-quality steel sheets of the multiphase microstructure. The obtained bainitic-austenitic and bainitic-martensitic microstructures (respectively for 3Mn-1.5Al-Nb and 5Mn-1.5Al-Nb steels) are characterized by the strong grain refinement both for laboratory and semi-industrial conditions. The successful production of the investigated steels require the increased flow stress, unit pressure and rolling load levels, which are independent on the Mn addition in a range from 3 to 5%. The detailed selection of strain, strain rate, deformation temperature and interpass time values have to be applied.

Acknowledgment

This publication was financed by the Ministry of Science and Higher Education of Poland as the statutory financial grant of the Faculty of Mechanical Engineering SUT.

REFERENCES

[1] N. Anand, S. Sankaran, R. Madhavan, S. Suwas, P. Venugopal, J. Mater. Eng. Perform. **24**, (1), 517-528 (2015).
[2] K. Radwański, Steel Res. Int. **86**, (11), 1379-1390 (2015).
[3] D. Krizan, B.C. De Cooman, Metall. Mater. Trans. A **45A**, 3481-3492 (2014).
[4] M. Adamczyk, D. Kuc, E. Hadasik, Arch. Civ. Mech. Eng. **8**, (3), 5-13 (2008).
[5] A. Kokosza, J. Pacyna, Mater. Sci. Technol. **31**, (7), 803-807 (2015).
[6] R.A. Mesquita, R. Schneider, K. Steineder, L. Samek, E. Arenholz, Metall. Mater. Trans. A **44**, (9), 4015-4019 (2013).
[7] M.B. Jabłońska, R. Michalik, Solid State Phenom. **227**, 109-112 (2015).
[8] A. Grajcar, M. Opiela, G. Fojt-Dymara, Arch. Civ. Mech. Eng. **9**, (3), 49-58 (2009).
[9] D. Kuc, E. Hadasik, G. Niewielski, I. Schindler, E. Mazancova, S. Rusz, P. Kawulok, Arch. Civ. Mech. Eng. **12**, (3), 312-317 (2012).
[10] L.A. Dobrzański, A. Grajcar, W. Borek, Mater. Sci. Forum **638-642**, 3224-3229 (2010).
[11] S. Lee, B.C. De Cooman, Metall. Mater. Trans. A **45**, (2), 709-716 (2014).
[12] A. Grajcar, R. Kuziak, Adv. Mater. Res. **314-316**, 119-122 (2011).
[13] A. Grajcar, K. Radwański, H. Krztoń, Solid State Phenom. **203-204**, 34-37 (2013).
[14] B. Garbarz, B. Niżnik-Harańczyk, Mater. Sci. Technol. **31**, (7), 773-780 (2014).
[15] E. Skołek. K. Wasiak, W.A. Świątnicki, Mater. Tehnol. **49**, 6, 933-939 (2015).
[16] K. Sugimoto, B. Yu, Y. Mukai, S. Ikeda, ISIJ Int. **45**, (8), 1194-1200 (2005).
[17] L.A. Dobrzański, M. Czaja, W. Borek, K. Labisz, T. Tański, Int. J. Mater. Prod. Tech. **51**, (3), 264-280 (2015).
[18] H. Jirkova, L. Kucerova, B. Masek, Mater. Sci. Forum **706-709**, 2734-2739 (2012).
[19] A. Lisiecki, Metals **5**, (1), 54-69 (2015).
[20] J.H. Park, D.J. Kim, D.J. Min, Metall. Mater. Trans. A **43**, 2316-2324 (2012).
[21] A. Grajcar, M. Kamińska, U. Galisz, L. Bulkowski, M. Opiela, P. Skrzypczyk, J. Achiev. Mater. Manuf. Eng. **55**, (2), 245-255 (2012).
[22] M. Opiela, J. Mater. Eng. Perform. **23**, (9), 3379-3388 (2014).
[23] K. Radwański, A. Wrożyna, R. Kuziak, Mater. Sci. Eng. A **639**,

567-574 (2015).
[24] A. Grajcar, P. Skrzypczyk, R. Kuziak, K. Gołombek, Steel Res. Int. **85**, (6), 1058-1069 (2014).
[25] B. Pereda, Z. Aretxabaleta, B. Lopez, J. Mater. Eng. Perform. **24**, (3), 1279-1293 (2015).
[26] F. Siciliano, L.L. Leduc, Mater. Sci. Forum **500-501**, 221-228 (2005).
[27] D. Liu, F. Fazeli, M. Militzer, W.J. Poole, Metall. Mater. Trans. A **38A**, 894-909 (2007).
[28] E. Hadasik, R. Kuziak, R. Kawalla, M. Adamczyk, M. Pietrzyk, Steel Res. Int. **77**, (12), 927-933 (2006).
[29] P. Uranga, B. Lopez, J.M. Rodriguez-Ibabe, Steel Res. Int. **78**, (3), 199-209 (2007).
[30] B. Garbarz, W. Burian, D. Woźniak, Steel Res. Int. Special issue, 1251-1254 (2012).
[31] A. Grajcar, P. Skrzypczyk, in: W. Bleck, D. Raabe (Eds.), Proc. of 2nd Int. Conf. on High Manganese Steel, 159-162, Aachen 2014.
[32] R.M. Skolly, E.I. Poliak, Mater. Sci. Forum **500-501**, 187-194 (2005).
[33] E.I. Poliak, D. Bhattacharya, Mater. Sci. Forum **783-786**, 3-8 (2014).
[34] A. Hensel, T. Spittel, Kraft- und Arbeitsbedarf Bildsamer Formgebungsverfahren, VEB Deutscher Verlag fur Grundstoffindustrie, Leipzig 1978.
[35] V.I. Zjuzin, M.J. Brovman, A.F. Melnikow, Soprotivlenije Deformacii Pro Goracej Prokatke, Metallurgija, Moskva 1964.
[36] H.J. Ha, C.J. Park, H.S. Kwon, Scripta Mater. **55**, (11), 991-994 (2006).
[37] A. Grajcar, W. Kwaśny, J. Achiev. Mater. Manuf. Eng. **54**, (2), 168-177 (2012).
[38] K.I. Sugimoto, H. Tanino, J. Kobayashi, Steel Res. Int. **86**, 1151-1160 (2015).